

EXOTIC BEHAVIOR OF HEXAGONS IN FARADAY WAVES

COMPORTAMIENTO EXÓTICO DE HEXÁGONOS EN ONDAS DE FARADAY

N. PÉRINET^a, D. JURIC^b AND L. S. TUCKERMAN^{c†}

a) Faculty of Science, University of Ontario Institute of Technology (UOIT), Oshawa, Ontario, Canada, L1H 7K4

b) LIMSI-CNRS (UPR 3251), B.P. 133, 91403 Orsay France

c) PMMH (UMR 7636 CNRS - ESPCI - UPMC - UPD), 10 rue Vauquelin, 75005 Paris France, laurette@pmmh.espci.fr[†]

† corresponding author

Three-dimensional numerical simulations of hexagonal patterns in Faraday waves are presented, including details of the velocity field and interface motion. The pattern does not remain hexagonal, but is succeeded by alternation of patterns we call quasi-hexagons and beaded stripes.

Se realizan simulaciones numéricas tridimensionales de patrones hexagonales en ondas de Faraday, incluyendo detalles del campo de velocidades y del movimiento de la interfaz. El patrón no permanece hexagonal, sino que es sustituido por patrones que llamaremos cuasi-hexagonales, alternando con patrones de bandas.

PACS: Symmetry breaking flow instabilities, 47.20.Ky; Flow instabilities interfacial, 47.20.Ma; Pattern formation in fluid dynamics 47.54.-r

In 1831, Faraday [1] observed that when a fluid layer is subjected to periodic vertical oscillation of sufficient amplitude, standing waves appear on its surface. These waves may take the form of regular stripes, squares, or hexagons. The experimental observation of more complicated structures, such as quasi-patterns, superlattices or oscillons in the 1990s, has led to a great deal of experimental and theoretical research. Numerical simulations are more recent: the first numerical simulation of Faraday waves was carried out in 2000 for the 2D case by Chen and Wu [2] and by Périnet *et al.* [3] in 2009 for the 3D case.

We summarize our formulation and the numerical methods used to compute the fluid motion; see [3] for a more detailed description. A single-fluid model is used to define the velocity \mathbf{u} and pressure p over the entire domain. The viscosity and density are variable, taking the values ν_1, ρ_1 for the denser fluid on the bottom, ν_2, ρ_2 for the lighter fluid at the top and varying abruptly at the surface. The equations we solve are then

$$\partial_t \mathbf{u} + (\mathbf{u} \cdot \nabla) \mathbf{u} = -\frac{1}{\rho} \nabla p + \nu \Delta \mathbf{u} - [g + a \sin(2\pi f t)] \mathbf{e}_z + \int \delta(\mathbf{x} - \mathbf{x}') \sigma \kappa \mathbf{n} dV \quad (1)$$

subject to the additional constraints of incompressibility $\nabla \cdot \mathbf{u} = 0$ and boundary conditions which are periodic in the horizontal directions and no-slip at the vertical boundaries. In (1), the additional gravitational term arises from the transformation to the oscillating reference frame of the container. The last term incorporates surface tension, with σ

the surface tension, κ the local curvature, \mathbf{n} the vector normal to the surface and pointing from the lower to the upper fluid, and \mathbf{x} and \mathbf{x}' the positions of points in the domain and on the interface.

We represent the velocity and pressure on a staggered MAC mesh [4] which is fixed and uniform. The moving interface, defined by $z = \zeta(x, y, t)$, is computed by a front-tracking [5]/immersed-boundary [6] method on a semi-Lagrangian triangular mesh which is fixed in the horizontal x and y directions and moves along the vertical direction z . The interface is advected and the density and viscosity fields updated. The capillary force is computed locally on the Lagrangian mesh and then incorporated into the Navier-Stokes equations, which are solved by a projection method. The Poisson problem for the pressure is solved via Biconjugate Gradient Stabilized (BiCGStab) iteration preconditioned by the inverse Laplacian.

The horizontal dimensions of the domain are chosen to accommodate a hexagonal pattern. We take $L_x = 2\lambda_c / \sqrt{3}$ and $L_y = 2\lambda_c$, so that large-scale spatial variations are inaccessible. The simulations were run with a spatial resolution of $N_x \times N_y \times N_z = 58 \times 100 \times 180$. Each horizontal rectangle is subdivided into 64 triangles to represent the interface. To validate the spatial discretization, we repeated the simulations with a finer resolution of $N_x \times N_y \times N_z = 75 \times 125 \times 225$. Although small quantitative changes were seen, the dynamics remained qualitatively unchanged. The time step is limited by the advective step, taking values varying

between T/24 000 and T/4000.

The first detailed spatio-temporal experimental measurements of the interface height of Faraday waves were undertaken by Kityk *et al.* [7, 8]. Their optical technique required the two fluid layers to have the same refractive index, which led them to use fluids of similar viscosities and densities: $\rho_1 = 1346 \text{ kg m}^{-3}$, $\nu_1 = 5.35 \times 10^{-6} \text{ m}^2 \text{ s}^{-1}$, $\rho_2 = 949 \text{ kg m}^{-3}$, $\nu_2 = 2.11 \times 10^{-5} \text{ m}^2 \text{ s}^{-1}$ and surface tension $\sigma = 35 \text{ mN m}^{-1}$. These parameters, especially the density ratio $\rho_2/\rho_1 = 0.7$, differ markedly from most studies of Faraday waves, which use air above either water or silicone oil and so have $\rho_2/\rho_1 \sim 0.001$. At rest, the heavy and light fluids occupy heights of $h_1 = 1.6 \text{ mm}$ and $h_2 = 8.4 \text{ mm}$, respectively. The imposed vibration has frequency $f = 12 \text{ Hz}$ and the Faraday instability leads to subharmonic standing waves, so that $\zeta(x, y, t)$ oscillates with period $T = 2/f = 0.1666 \text{ s}$. Floquet analysis [9] for these parameters yields a critical wavelength of $\lambda_c = 2\pi / k_c = 13.2 \text{ mm} \gg h_1$, so that the fluid layer is quite shallow.

The critical acceleration obtained by Floquet analysis is $a_c = 25.8 \text{ ms}^{-2} = 2.63g$. For $a \gtrsim a_c$, square patterns are observed experimentally and numerically [3, 7, 8]. The simulations described here were carried out at higher acceleration, $a = 38.0 \text{ ms}^{-2} = 3.875g = 1.473 a_c$, starting from zero velocity and an initial randomly perturbed interface. The simulations produced a hexagonal pattern which oscillates subharmonically [3, 7, 8]. Visualizations of representative velocity fields and of the interface throughout an oscillation period are shown in figures 1 and 2. The patterns and their evolution are far from trigonometric in space and in time. The temporal anharmonicity is a consequence of the high viscosity: a high vibration amplitude a is necessary to overcome the damping and so equation (1) is far from homogeneous in time. The spatial anharmonicity is due in part to the fact that the hexagonal pattern succeeds the squares which appear at onset.

After about 10 subharmonic periods, the hexagonal symmetry is broken and the pattern is replaced, first by another pattern we call beaded stripes, and then by alternation between patterns we call quasi-hexagons and nonsymmetric beaded stripes. Figure 3 shows the time evolution of the instantaneous maximum height $\max_{x,y} \zeta(x, y, t)$ and its envelope $\max_{x,y,[t,t+T]} \zeta(x, y, t)$. Surrounding the time-evolution plot are contour plots of the instantaneous interface height at representative times over one subharmonic cycle, i.e. at times $t_i + jT/4$ for $j=0, \dots, 3$. The maximum height is strongly correlated with the flow pattern. Since the spatial average of the height remains constant, its maximum measures the spatial variation of the interface. Hexagons (t_1) have the highest peaks, followed by quasi-hexagons (t_3, t_5), and then by beaded stripes (t_2, t_4, t_6). The hexagonal patterns are invariant under the usual symmetry operations of rotation by $\pi/3$ and reflection. The beaded striped patterns are instead invariant under the two reflections:

$$\zeta(x, y) = \zeta(x, n\lambda_c - y) \quad (2a)$$

$$\zeta(x, y) = \zeta(m\lambda_c / \sqrt{3} + \tilde{x}_0 - x, y + n\lambda_c) \quad (2b)$$

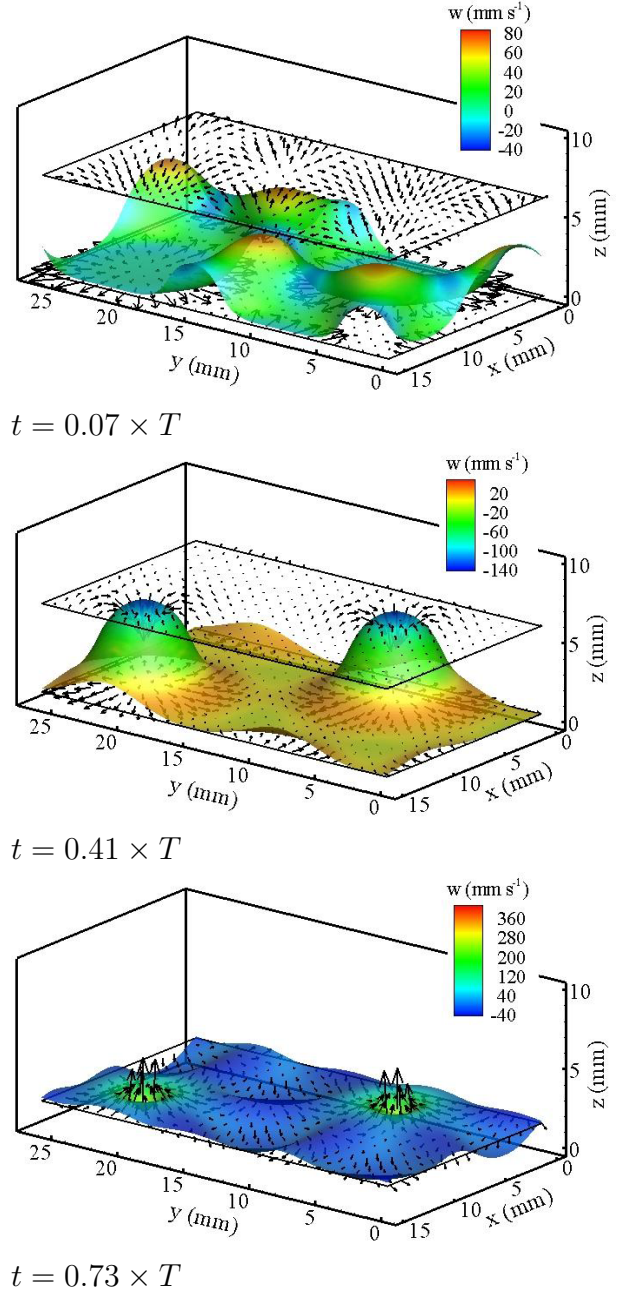


Figure 1: Velocity fields associated with hexagonal patterns.

The quasi-hexagons and nonsymmetric beaded stripes have no exact symmetries but they obey the spatio-temporal symmetry

$$\zeta(x, y, t_{3,6}) = \zeta(m\lambda_c / \sqrt{3} + x_0 - x, y + y_0, t_{3,4} + T/2) \quad (3)$$

That is, the quasi-hexagonal pattern at t_3 is related by a spatial shift-and-reflect operation to that at $t_5 + T/2$ and similarly for the beaded striped patterns at t_4 and t_6 . In (2)-(3), \tilde{x}_0 , x_0 and y_0 are spatial phases whose values depend on details of the initial condition.

The long-time behavior seen in figure 3 could consist of trajectories connecting quasi-hexagonal and beaded striped patterns of each of two phases, i.e. a heteroclinic cycle. An investigation of this hypothesis is currently underway.

[1] M. Faraday, Phil. Trans. R. Soc. Lond. **121**, 299 (1831).
 [2] P. Chen and K.-A. Wu, Phys. Rev. Lett. **85**, 3813 (2000).
 [3] N. Périnet, D. Juric and L. S. Tuckerman, J. Fluid Mech. **635**, 1 (2009).
 [4] F. H. Harlow and J. E. Welch, Phys. Fluids **8**, 2182 (1965).
 [5] G. Tryggvason, B. Bunner, A. Esmaeeli, D. Juric, N. Al-Rawahi, W. Tauber, J. Han and Y.-J. Jan, J. Comput. Phys. **169**,

708 (2001).
 [6] C. S. Peskin, J. Comput. Phys. **25**, 220 (1977).
 [7] A. V. Kityk, J. Embs, V. V. Mekhonoshin and C. Wagner, Phys. Rev. E **72**, 036209 (2005).
 [8] A. V. Kityk, J. Embs, V. V. Mekhonoshin and C. Wagner, Phys. Rev. E **79**, 029902 (2009).
 [9] K. Kumar and L. S. Tuckerman, J. Fluid. Mech. **279**, 49 (1994).

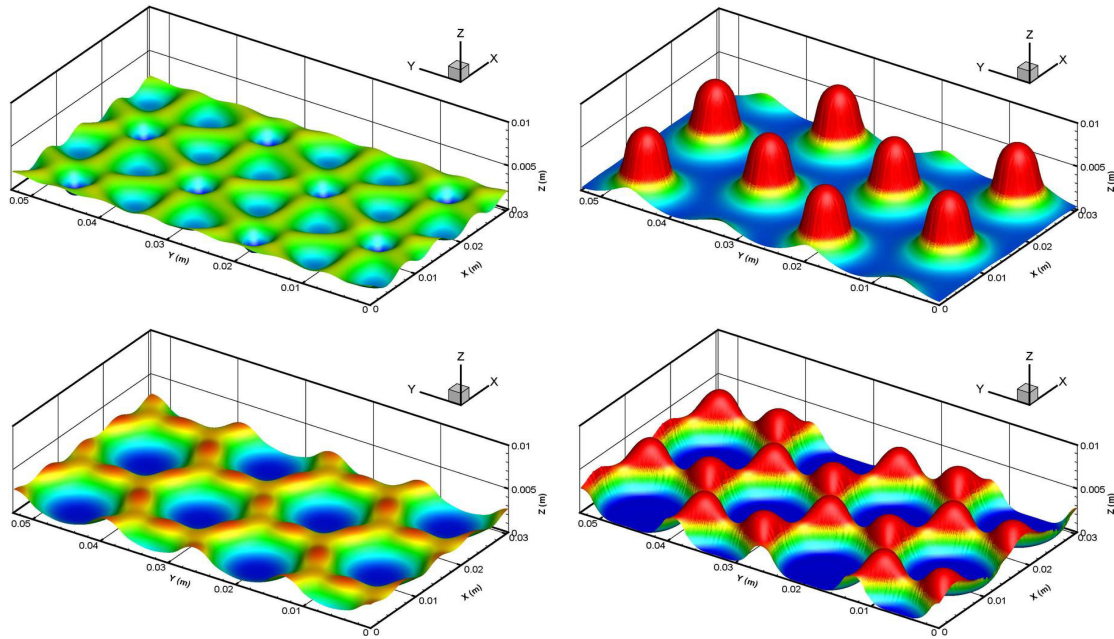


Figure 2: Visualizations of hexagonal interface over one subharmonic oscillation period. The size of the visualization domain is double that of the computational domain in each direction.

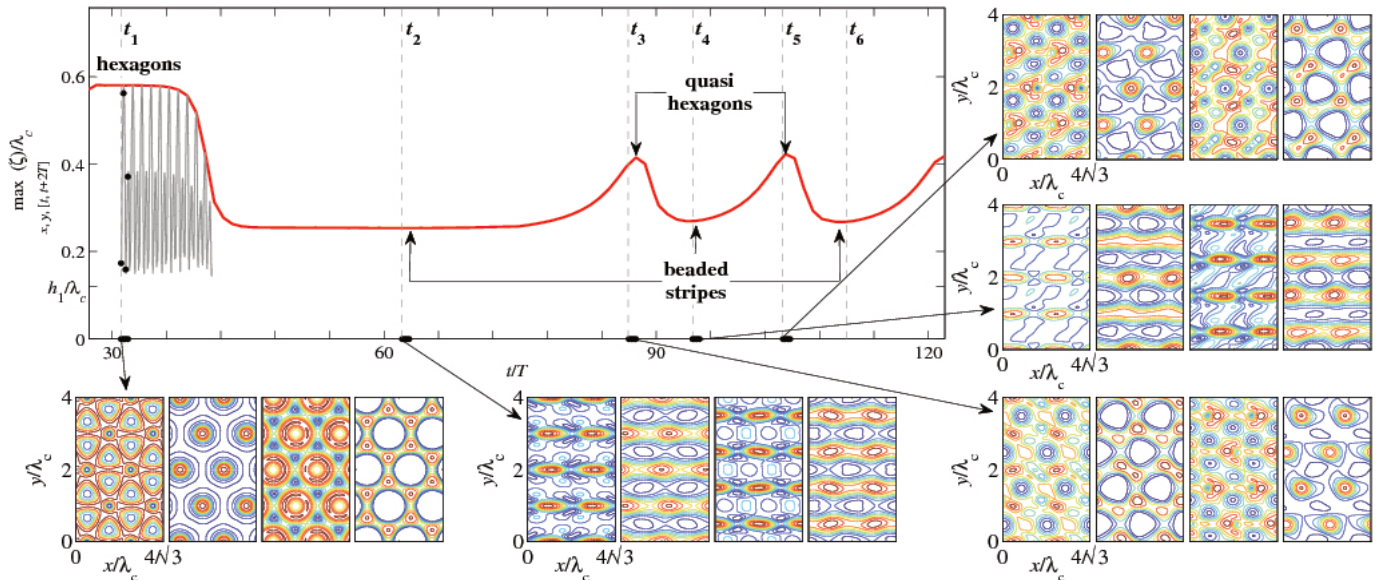


Figure 3: Maximum interface heights $\max_{x,y} \zeta(x,y,t)$ (rapidly oscillating curve) and $\max_{x,y,[t,t+T]} \zeta(x,y,t)$ (smooth curve). Surrounding visualizations show instantaneous contour plots of $\zeta(x,y,t)$. The size of the box has been doubled in each dimension. Visualizations shown at $t_i + jT/4$ for $j = 0, 1, 2, 3$, i.e. over one subharmonic period. The hexagonal patterns at time t_1 can be compared with the three-dimensional visualizations shown in figure 3. The pattern consists of beaded stripes at time t_2 , quasi-hexagons at t_3 and t_5 , and nonsymmetric beaded stripes at t_4 and t_6 . Over the large white areas, the interface is very close to the bottom and almost flat. Patterns at t_3 and t_5 , and at t_4 and t_6 are related by the spatio-temporal transformation (3).